Experimental assessment of mixed-mode partition theories

Experimental assessment of mixed-mode partition theories

C. M. Harvey and S. Wang*

Department of Aeronautical and Automotive Engineering, Loughborough University, Loughborough, Leicestershire LE11 3TU, UK

Abstract

The propagation of mixed-mode interlaminar fractures is investigated using existing experimental results from the literature and various partition theories. These are (i) a partition theory by Williams (1988) based on Euler beam theory; (ii) a partition theory by Suo (1990) and Hutchinson and Suo (1992) based on 2D elasticity; and (iii) the Wang-Harvey partition theories of the authors based on the Euler and Timoshenko beam theories. The Wang-Harvey Euler beam partition theory seems to offer the best and most simple explanation for all the experimental observations. No recourse to fracture surface roughness or new failure criteria is required. It is in excellent agreement with the linear failure locus and is significantly closer than other partition theories. It is also demonstrated that the global partition of energy release rate when using the Wang-Harvey Timoshenko beam or averaged partition theories or 2D elasticity exactly corresponds with the partition from the Wang-Harvey Euler beam partition theory. It is therefore concluded that the excellent performance of the Wang-Harvey Euler beam partition theory is either due to the failure of materials generally being based on global partitions or that for the specimens tested, the through-thickness shear effect is negligibly small. Further experimental investigations are definitely required.

Keywords: Composite materials, Failure criterion, Interlaminar fracture, Mixed-mode tests, Mixed-mode partition, Spalling

1. Introduction

In brittle, isotropic, homogeneous materials, it is well known that cracks propagate under pure mode I conditions [1,2]. The direction of propagation is determined by the need to maintain these conditions. This is known as the 'criterion of local symmetry'. However, in cases where cracks exist between interfaces, cracks are often constrained to propagate along these interfaces because they represent a plane of weakness. Fibre-reinforced composite laminates are examples of such materials. They are highly inhomogeneous and anisotropic. In these materials, interface cracks correspond to delaminations. In this paper, delaminations are simply referred to as 'fractures' or 'cracks' in order to keep consistency with the description of fracture mechanics. In interface cracking, cracks generally propagate as a mixed mode and can even propagate under pure mode II loading. Since materials have different fracture toughness in each mode, fracture mode partitions play a key role in the propagation of fractures and in the development of crack propagation criteria.

* Corresponding Author
Email addresses: s.wang@lboro.ac.uk (S. Wang), c.m.harvey@lboro.ac.uk (C. Harvey)

NOMENCLATURE

a	length of fracture
A_1, A_2, A	extensional stiffness of upper, lower and intact beams
b	beam width
B_1, B_2, B	coupling stiffness of upper, lower and intact beams
D_1, D_2, D	bending stiffness of upper, lower and intact beams
E	Young's modulus
G, G_I, G_{II}	total, mode I and mode II energy release rates
G_c, G_{Ic}, G_{IIc}	total, mode I and mode II critical energy release rates
G_{xz}	shear modulus
h_1, h_2, h	thicknesses of upper, lower and intact beams
I_1, I_2, I	second moments of area of upper, lower and intact beams
K, K_I, K_{II}	total, mode I and mode II stress intensity factors
K_{Ic}, K_{IIc}	total, mode I and mode II critical stress intensity factors
M_1, M_2	bending loads acting on upper and lower beams
M_{1B}, M_{2B}, M_B	bending moments on upper, lower and intact beams at the crack tip
N_1, N_2	axial loads acting on upper and lower beams
N_{1B}, N_{2B}, N_B	axial forces on upper, lower and intact beams at the crack tip
β, β'	pure mode II relationships from the first and second set respectively
γ	thickness ratio h_2/h_1
θ, θ'	pure mode I relationships from the first and second set respectively
ξ	non-dimensional crack-depth coefficient in spalling
Φ	crack loading coefficient in spalling

Abbreviations

CLT	classical lamination theory
DCB	double cantilever beam
ELS	end-loaded split
ENF	end-notched flexure
FEM	finite element method
FRMM	fixed-ratio mixed-mode
MMB	mixed-mode bending
PEEK	Polyether ether ketone
QUAD4	four-node quadrilateral with linear displacement field

The problem of interface cracking has been studied extensively using varied approaches. Broadly the work can be categorised as analytical, numerical or experimental. In this work, the performance of a number of analytical partition theories is investigated by comparing their predictions with experimental results available in the literature.

Some of the earliest analytical work was carried out by Williams [3], who made significant contributions to the understanding. He successfully identified one pair of pure mode conditions (mode I and mode II), which are valid for Euler double cantilever beams (DCBs) with bending moments alone. Unfortunately, the other set of pure mode conditions and the stealthy interactions between pure modes were missed in his work. As a result, his partition theory is only able to give the correct partition for symmetric DCBs. Another piece of pioneering work [4] was given by Schapery and Davidson, which is also for DCBs based on Euler beam theory. This partition theory is not able to give the Williams pair of pure modes [3] and is a combined numerical and analytical theory. Schapery and Davidson also claimed that Euler beam theory did not provide quite enough information to obtain a decomposition of energy release rate into opening and shearing mode components. Suo [5], Suo and Hutchinson [6] and Hutchinson and Suo [7] developed a partition theory for isotropic DCBs using 2D elasticity and stress intensity factors, which are analytical except for one parameter, which is determined numerically. Ref. [7] reported that Ref. [3] contained conceptual errors. Bruno and Greco [8] presented an analytical mode-partitioning theory for bi-layered Euler beams. They correctly identified a couple of pure modes but unfortunately they missed the stealthy interactions. Therefore the partition is in error. Several recent research works on the topic are quoted here among many others. They are Wang and Qiao [9], Nguyen and Levy [10], Yan and Shang [11], Ouyang and Li [12] and Zou et al. [13,14].

Recently the authors have developed completely analytical theories for one-dimensional fractures in straight beams and axisymmetric plates made of either isotropic or laminated composite materials. These theories are based on the classical and first-order shear deformable beam and plate theories. The work has been reported on several occasions [15-19]. Full details are available in Refs. [19-21]. In these theories, two sets of pure mode pairs were identified. In the Wang-Harvey Euler beam partition theory, the two sets of pure mode pairs are distinct and this leads to stealthy interactions. Under the Wang-Harvey Timoshenko beam partition theory, the two sets of pure mode pairs exactly coincide and there are no stealthy interactions. It was also found that the average of these two extreme cases provides a very accurate approximation to the 2D elasticity result from the Suo-Hutchinson partition theory [5-7]. The theories were validated through extensive numerical simulations.

On the experimental front, some early work is given by Thouless [22] and Thouless et al. [23]. These works looked at interfacial failure under mixed-mode loading and the spalling of brittle plates, respectively. The latter reference makes comparisons between the experimental results and the Suo-Hutchinson partition theory [5-7]. Many other experimental investigations make use of Williams' partition theory [3] to set up test apparatus and to partition the experimentally measured energy release rate [24-28].

In this work, a number of existing analytical partition theories, namely the Williams [3], the Suo-Hutchinson [5-7] and the Wang-Harvey [19-21] partition theories are assessed using results from the various experimental tests described in the literature. The original contribution of this paper is to assess the relative performance of each theory in predicting the experimental observations. The performance of the Wang-Harvey theories has not been assessed in this manner before. Validation of the Wang-Harvey theories has only been carried out with numerical results from the finite element method (FEM). Experimental validation of these theories is also very important. In addition, the final expressions for energy release rate partition in the Wang-Harvey theories [19-21] are presented in a more convenient format for usage.

The structure of the paper is as follows. The different partition theories are given in Section 2. A discussion on and insights into the differences between local and global partitioning is given in Section 3. This has been the subject of much discussion in the literature [25-27]. In Section 4, data from the various experimental tests described in the literature is analysed using the different partition theories. Finally, conclusions are given in Section 5.

2. Mixed-mode partition theories

2.1. The Wang-Harvey partition theories

The Wang-Harvey partition theories are for one-dimensional fractures in straight beams and axisymmetric plates made of either isotropic or laminated composite materials [19-21]. Full details of the theories are given in Refs [19-21]. In this paper, only the final expressions for energy release rate partition are presented in a format, which is considered the most convenient for use by academic researchers and industrial engineers. In previous work [19-21], they have been presented in a format, which is most revealing of the underlying mechanics.

Fig. 1 (a) shows a DCB with its associated geometry, two tip bending moments, and two tip axial forces. The partition is based on the bending moments and axial forces acting at the crack tip B, which are shown in Fig. 1 (b). According to the Wang-Harvey Euler beam partition theory [19-21], the mode I and II components of the total energy release rate, denoted by G_{IE} and G_{IIE} respectively, are

$$G_{IE} = c_{IE}\left(M_{1B} - \frac{M_{2B}}{\beta_1} - \frac{N_{1B}}{\beta_2} - \frac{N_{2B}}{\beta_3}\right)\left(M_{1B} - \frac{M_{2B}}{\beta_1'} - \frac{N_{1B}}{\beta_2'} - \frac{N_{2B}}{\beta_3'}\right) \tag{1}$$

$$G_{IIE} = c_{IIE}\left(M_{1B} - \frac{M_{2B}}{\theta_1} - \frac{N_{1B}}{\theta_2} - \frac{N_{2B}}{\theta_3}\right)\left(M_{1B} - \frac{M_{2B}}{\theta_1'} - \frac{N_{1B}}{\theta_2'} - \frac{N_{2B}}{\theta_3'}\right) \tag{2}$$

where θ_i and β_i represent the first set of pure mode I and II relationships respectively and θ_i' and β_i' represent the second set [19-21]. They are recorded here.

$$\theta_1 = \frac{\left(B_2^2 - A_2 D_2\right)\left(B_1 + h_1 A_1/2\right)}{\left(B_1^2 - A_1 D_1\right)\left(B_2 - h_2 A_2/2\right)} \tag{3}$$

$$\theta_2 = -\frac{B_1 + h_1 A_1/2}{D_1 + h_1 B_1/2} \tag{4}$$

$$\theta_3 = \frac{\left(B_1 + h_1 A_1/2\right)\left(B_2^2 - A_2 D_2\right)}{\left(D_2 - h_2 B_2/2\right)\left(B_1^2 - A_1 D_1\right)} \tag{5}$$

$$\beta_1 = -\frac{D_2^*\left(D_1^* + D_1^{**}\theta_1 - D^*\right)}{D_1^*\left(D_2^* + D_2^*\theta_1 - D^*\theta_1\right)} \tag{6}$$

$$\beta_2 = \frac{\theta_2\left(\frac{h_2}{2D^*} - \frac{B_1}{B_1^*} + \frac{B}{B^*}\right) + \frac{1}{D_1^*} - \frac{1}{D^*}}{\theta_2\left(\frac{Bh_2}{B^*} - \frac{1}{A_1^*} + \frac{1}{A^*} + \frac{h_2^2}{4D^*}\right) - \frac{h_2}{2D^*} + \frac{B_1}{B_1^*} - \frac{B}{B^*}} \tag{7}$$

$$\beta_3 = \frac{\theta_3\left(\frac{h_1}{2D^*} - \frac{B}{B^*}\right) - \frac{1}{D_1^*} + \frac{1}{D^*}}{\theta_3\left(\frac{Bh_1}{B^*} + \frac{1}{A_2^*} - \frac{1}{A^*} - \frac{h_1^2}{4D^*}\right) - \frac{h_1}{2D^*} + \frac{B}{B^*}} \tag{8}$$

$$\theta_1' = -1 \tag{9}$$

$$\theta_2' = \frac{\beta_2'\left(\frac{h_2}{2D^*} - \frac{B_1}{B_1^*} + \frac{B}{B^*}\right) + \frac{1}{D_1^*} - \frac{1}{D^*}}{\beta_2'\left(\frac{Bh_2}{B^*} - \frac{1}{A_1^*} + \frac{1}{A^*} + \frac{h_2^2}{4D^*}\right) - \frac{h_2}{2D^*} + \frac{B_1}{B_1^*} - \frac{B}{B^*}} \tag{10}$$

$$\theta_3' = \frac{\beta_3'\left(\frac{h_1}{2D^*} - \frac{B}{B^*}\right) - \frac{1}{D_1^*} + \frac{1}{D^*}}{\beta_3'\left(\frac{Bh_1}{B^*} + \frac{1}{A_2^*} - \frac{1}{A^*} - \frac{h_1^2}{4D^*}\right) - \frac{h_1}{2D^*} + \frac{B}{B^*}} \tag{11}$$

$$\beta_1' = \frac{D_2^*}{D_1^*} \tag{12}$$

$$\beta_2' = -\frac{A_1}{B_1} \tag{13}$$

$$\beta_3' = -\frac{B_2^*}{D_1^* B_2} \tag{14}$$

The remaining variables in Eqs. (1) and (2) are

$$c_{HE} = G_{\theta_1}\left[\left(1 - \frac{\theta_1}{\beta_1}\right)\left(1 - \frac{\theta_1}{\beta_1'}\right)\right]^{-1} \tag{15}$$

$$c_{HE} = G_{\beta_1}\left[\left(1 - \frac{\beta_1}{\theta_1}\right)\left(1 - \frac{\beta_1}{\theta_1'}\right)\right]^{-1} \tag{16}$$

where

$$G_{\theta_1} = \frac{1}{2b^2}\left[\frac{1}{D_1^*} + \frac{\theta_1^2}{D_2^*} - \frac{\left(1+\theta_1\right)^2}{D^*}\right] \tag{17}$$

$$G_{\beta_1} = \frac{1}{2b^2}\left[\frac{1}{D_1^*} + \frac{\beta_1^2}{D_2^*} - \frac{\left(1+\beta_1\right)^2}{D^*}\right] \tag{18}$$

The extensional, coupling and bending stiffness are denoted by A, B and D respectively. Note that these quantities take different values under the plane-strain assumption from those under the plane-stress assumption. Readers are referred to Li's work [29,30] for details. However, there is no difference between the two assumptions in the following development.

$$A_i^* = A_i - B_i^2 / D_i \tag{19}$$

$$B_i^* = B_i^2 - A_i D_i \tag{20}$$

$$D_i^* = D_i - B_i^2 / A_i \tag{21}$$

The range of i is 1 and 2, which refers to the upper and lower sub-laminates respectively. No subscript is used for the intact part of the laminate. A_1 is therefore the extensional stiffness of the upper beam and A is the extensional stiffness of the intact beam, etc.

According to the Wang-Harvey Timoshenko beam partition theory [19-21], the mode I and II components of the energy release rates denoted by G_{IT} and G_{IIT} respectively are

$$G_{II} = c_{IT}\left(M_{1B} - \frac{M_{2B}}{\beta_1} - \frac{N_{1B}}{\beta_2} - \frac{N_{2B}}{\beta_3}\right)^2 \tag{22}$$

$$G_{IIT} = c_{IIT}\left(M_{1B} - \frac{M_{2B}}{\theta_1} - \frac{N_{1B}}{\theta_2} - \frac{N_{2B}}{\theta_3}\right)^2 \tag{23}$$

where

$$c_{IT} = G_{\theta_1}\left(1 - \frac{\theta_1}{\beta_1}\right)^{-2} \tag{24}$$

$$c_{IIT} = G_{\beta_1}\left(1 - \frac{\beta_1}{\theta_1}\right)^{-2} \tag{25}$$

Finally, the averaged partition theory is the average of the Wang-Harvey Euler and Timoshenko beam partitions. This partition has been found to give an excellent approximation to the partition from 2D elasticity [19-21]. The mode I and II components of the energy release rate from the averaged partition theory are denoted by G_{IA} and G_{IIA} respectively. They are

$$G_{IA} = \left(G_{IE} + G_{IT}\right)/2 \tag{26}$$

$$G_{IIA} = \left(G_{IIE} + G_{IIT}\right)/2 \tag{27}$$

These three partitions are easily reduced for isotropic materials [19,20]. A thickness ratio $\gamma = h_2/h_1$ is now introduced. The present Euler beam partitions for isotropic beams reduce to [19,20]

$$G_{IIE} = c_{IIE}\left(M_{1B} - \frac{M_{2B}}{\beta_1} - \frac{N_{1Bc}}{\beta_2}\right)\left(M_{1B} - \frac{M_{2B}}{\beta_1'}\right) \tag{28}$$

$$G_{IIE} = c_{IIE}\left(M_{1B} - \frac{M_{2B}}{\theta_1} - \frac{N_{1Bc}}{\theta_2}\right)\left(M_{1B} - \frac{M_{2B}}{\theta_1'} - \frac{N_{1Bc}}{\theta_2'}\right) \tag{29}$$

where c_{IIE} and c_{IIE} are still given by Eqs. (15) and (16) and

$$N_{1Bc} = N_{1B} - N_{2B}/\gamma \tag{30}$$

The pure mode relationships are now as follows:

$$\theta_1 = -\gamma^2 \tag{31}$$

$$\theta_2 = -\frac{6}{h_1} \tag{32}$$

$$\beta_1 = \frac{\gamma^2\left(3+\gamma\right)}{1+3\gamma} \tag{33}$$

$$\beta_2 = \frac{2\left(3+\gamma\right)}{h_1\left(\gamma-1\right)} \quad \text{for} \quad \gamma \neq 1 \tag{34}$$

$$= 1 \quad \text{for} \quad \gamma = 1$$

$$\theta_1' = -1 \tag{35}$$

$$\theta_2' = -\frac{6\left(1+\gamma\right)}{h_1\left(1+\gamma^3\right)} \tag{36}$$

$$\beta_1' = \gamma^3 \tag{37}$$

The isotropic G_{θ_1} and G_{β_1} for use in Eqs. (15) and (16) are

$$G_{\theta_1} = \frac{24\gamma}{Eb^2h_1^3\left(1+\gamma\right)} \tag{38}$$

$$G_{\beta_1} = \frac{72\gamma\left(1+\gamma\right)}{b^2Eh_1^3\left(1+3\gamma\right)^2} \tag{39}$$

The present Timoshenko beam partitions for isotropic beams reduce to [19,20]

$$G_{IT} = c_{IT}\left(M_{1B} - \frac{M_{2B}}{\beta_1} - \frac{N_{1Bc}}{\beta_2}\right)^2 \tag{40}$$

$$G_{IIT} = c_{IIT}\left(M_{1B} - \frac{M_{2B}}{\theta_1} - \frac{N_{1Bc}}{\theta_2}\right)^2 \tag{41}$$

where c_{IT} and c_{IIT} are given by Eqs. (24) and (25). The averaged partition is obviously still given by Eqs. (26) and (27).

Finally, the present partition theories are presented for the special case of spalling (sub-surface cracks), where $\gamma \to \infty$. The present partitions using the Euler beam, Timoshenko beam and averaged fracture mode partition theories are respectively

$$G_{IE} = \frac{3M_{1B}\left(2M_{1B} - h_1 N_{1B}\right)}{b^2 h_1^3 E} \quad \text{and} \quad G_{IIE} = \frac{\left(6M_{1B} + N_{1B}h_1\right)\left(6M_{1B} + 5h_1 N_{1B}\right)}{16b^2 h_1^3 E} \tag{42}$$

$$G_{IT} = \frac{3\left(2M_{1B} - h_1 N_{1B}\right)^2}{8b^2 h_1^3 E} \quad \text{and} \quad G_{IIT} = \frac{\left(6M_{1B} + h_1 N_{1B}\right)^2}{8b^2 h_1^3 E} \tag{43}$$

$$G_{IA} = \frac{3\left(2M_{1B} - h_1 N_{1B}\right)\left(10M_{1B} - h_1 N_{1B}\right)}{16b^2 h_1^3 E}$$
$$\text{and} \quad G_{IIA} = \frac{\left(6M_{1B} + h_1 N_{1B}\right)\left(6M_{1B} + 5h_1 N_{1B}\right)}{16b^2 h_1^3 E} \tag{44}$$

The total energy release rate G is the same for all three theories

$$G = \frac{12M_{1B}^2 + h_1^2 N_{1B}^2}{2b^2 h_1^3 E} \tag{45}$$

Note that for the tests considered in this paper, the through-thickness shear effect due to applied shear forces is small and is safely ignored. Also in these tests, contact between the upper and lower beams is not a concern and so the contact behaviour is only briefly described here. For Timoshenko beams, crack tip running contact occurs, which results in pure mode II fractures. For Euler beams, the contact behaviour depends on the relative geometric and material properties of the upper and lower beams and the mode partition can either be pure mode II or mixed. Contact has been considered in full detail in previous work by the authors [20,21].

2.2. The Suo-Hutchinson partition theory

Suo and Hutchinson [5-7] considered a crack in a semi-infinite strip of orthotropic material and derived expressions for the mixed-mode intensity factors, which are analytical except for one parameter, which is determined numerically. Good agreement between the Suo-Hutchinson partition theory and the averaged partition theory has been observed [19-20]. This partition is now reproduced here. For consistency, the notation has been changed where appropriate to match the conventions used elsewhere in this paper. This partition theory assumes that a square-root singular field exists, so the partition is expressed in terms of stress intensity factors. The mode I and II stress intensity factors K_{ISH} and K_{IISH} are

$$K_{ISH} = \frac{N}{\sqrt{2h_1 U}}\cos\left(\omega\right) + \frac{M}{\sqrt{2h_1^3 V}}\sin\left(\omega+\varepsilon\right) \tag{46}$$

$$K_{IISH} = \frac{N}{\sqrt{2h_1 U}}\sin\left(\omega\right) - \frac{M}{\sqrt{2h_1^3 V}}\cos\left(\omega+\varepsilon\right) \tag{47}$$

where M and N are linear combinations of the applied loads:

$$bN = -N_1 + C_1\left(N_1 + N_2\right) - C_2\left[M_1 + M_2 + \frac{h_1}{2}\left(N_2 - \gamma N_1\right)\right]\Big/ h_1 \tag{48}$$

$$bM = M_1 - C_3\left[M_1 + M_2 + \frac{h_1}{2}\left(N_2 - \gamma N_1\right)\right] \tag{49}$$

$$C_1 = \frac{1}{1+\gamma} \quad \text{and} \quad C_2 = \frac{6\gamma}{\left(1+\gamma\right)^3} \quad \text{and} \quad C_3 = \frac{1}{\left(1+\gamma\right)^3} \tag{50}$$

The geometric factors U, V and ε are functions of γ:

$$U = \frac{\gamma^3}{3+6\gamma+4\gamma^2+\gamma^3} \quad \text{and} \quad V = \frac{\gamma^3}{12\left(1+\gamma^3\right)} \quad \text{and} \quad \frac{\sin\varepsilon}{\sqrt{UV}} = \frac{6\left(1+\gamma\right)}{\gamma^3} \tag{51}$$

The quantity ω is determined from the following approximate formula:

$$\omega = 52.1^\circ - 3^\circ/\gamma \tag{52}$$

For the spalling case, taking the limit where $\gamma \to \infty$, gives

$$K_{ISH} = \frac{M_1}{b}\sqrt{\frac{6}{h_1^3}}\sin\left(52.1^\circ\right) - \frac{N_1}{b}\sqrt{\frac{2}{h_1}}\cos\left(52.1^\circ\right) \tag{53}$$

$$K_{IISH} = -\frac{M_1}{b}\sqrt{\frac{6}{h_1^3}}\cos\left(52.1^\circ\right) - \frac{N_1}{b}\sqrt{\frac{1}{2h_1}}\sin\left(52.1^\circ\right) \tag{54}$$

For comparison with the energy release rates from the beam theories, the relationship between energy release rate and stress intensity factor for plane stress is

$$K^2 = EG \tag{55}$$

Again, for plane strain, E may simply be replaced by $E/\left(1-\nu^2\right)$.

2.3. The Williams partition theory

Williams was one of the first researchers to attempt to partition a mixed mode [3]. His theory has been applied to the various test methods for laminates [3,24,25]. Some work has been also been done to experimentally assess the performance of the theory [25-27]. His pioneering work was partially successful, in that this theory correctly predicts a pair of pure modes and can also give the correct partition for a symmetric DCB, i.e. $\gamma = 1$. However, it cannot identify the other

pure modes and missed the stealthy interactions between pure modes [18-20]. The limitations have been reported many times and by several different researchers [7,20].

The Williams partition, denoted by G_{IW} and G_{IIW}, is now reproduced here. Again, for consistency, the notation has been changed where appropriate to match the conventions in this paper.

$$G_{IW} = \frac{6\left(M_{2B} - M_{1B}\gamma^3\right)^2}{b^2 h_1^3 E\gamma^3\left(1+\gamma^3\right)} \tag{56}$$

$$G_{IIW} = \frac{18\gamma\left(M_{1B} + M_{2B}\right)^2}{b^2 E h_1^3\left(1+\gamma\right)^3\left(1-\gamma+\gamma^2\right)} + \frac{\left(1-\gamma\right)^2\left(N_{2B} - \gamma N_{1B}\right)^2}{2b^2 h_1 E\gamma^3\left(1+\gamma\right)} \tag{57}$$

For the spalling case, taking the limit where $\gamma \to \infty$, gives

$$G_{IW} = \frac{6M_{1B}^2}{b^2 h_1^3 E} \quad \text{and} \quad G_{IIW} = \frac{N_{1B}^2}{2b^2 h_1 E} \tag{58}$$

3. Nature of local and global partitions

There is an important difference between a local partition and a global partition. Simply put, local pureness is defined with respect to the crack tip B whilst the global pureness is defined with respect to the Δa region (shown in Fig. 1), which is the region mechanically affected by the presence of the crack. Mathematically, the difference is in the integration limits of the crack closure integral: the global partition is calculated by including the whole crack influence region in the integration limits; the local partition only considers the near-crack tip region. Note that the total energy release rate is not affected by the limits of the crack closure integral [31], however the partition of energy release rate is affected [20,21] and this will be further demonstrated and explained later in this section by numerical means. Full analytical details are available in Refs. [20,21].

It has been mathematically shown by the authors [20,21] that the Wang-Harvey Euler beam partition theory has two sets of pure modes (the first θ_i, β_i set and the second θ_i', β_i' set), which are both locally and globally pure. The local and global partitions are therefore the same when using the Wang-Harvey Euler beam partition theory. For the Wang-Harvey Timoshenko beam partition theory, there are two sets of locally pure modes, which exactly coincide on the first θ_i, β_i set from the Wang-Harvey Euler beam partition theory. There are also two sets of globally pure modes and they are the same as the pure modes from the Wang-Harvey Euler beam partition theory. Therefore, when using the Wang-Harvey Timoshenko beam partition theory, the local partition exhibits no stealthy interaction (because the two sets of local pure modes coincide) and is different to the Wang-Harvey Euler beam partition theory. However, the global partition is the *same* as the Wang-Harvey Euler beam partition theory. Since the averaged partition theory is the average of the Wang-Harvey Euler and Timoshenko beam partition theories, it behaves in the same way. The global partition is the same as the Wang-Harvey Euler beam partition theory but the local partition is generally different. Note that in all the cases discussed, the θ_i, β_i set of pure modes is always both locally and globally pure. This is why it provides the complete basis for mode partitioning.

This difference between local and global partitions is important because it is not known which is more appropriate for determining fracture propagation between interfaces and under what circumstances. In the following section, published experimental data will be used to try to make an assessment of this.

It is simple to show that the Wang-Harvey *global* Timoshenko beam and averaged partition theories are the same as the Wang-Harvey Euler beam partition theory. The authors have developed an FEM simulation capability, which is based on the Euler and Timoshenko beam theories and 2D elasticity. Normal and shear point interface springs with very high stiffness are used to model perfectly bonded plies. The energy release rate partition is calculated using the virtual crack closure technique in conjunction with these interface springs [32-35]. The number of spring pairs used in the calculation of energy release rate can easily be adjusted, from one spring pair for the local partition to many spring pairs to approach the global partition.

Numerical tests were carried out on the DCB shown in Fig. 1 (a). The Young's modulus is $E = 1$, the Poisson's ratio is $\nu = 0.3$ and the shear modulus is $G_{xz} = E/\left[2\left(1+\nu\right)\right] = 1/2.6$. The intact length is $L = 100$, the crack length is $a = 10$ and the width is $b = 1$. The thickness is $h = h_1 + h_2 = 3$ with $h_1 = 1$. Therefore, the thickness ratio is $\gamma = 2$. The DCB is under tip bending moments $M_1 = 1$ and M_2 which varies from -10 to 10. There are no axial forces or shear forces in this example. An interface spring stiffness of $k_s = 10^6$ was used for a rigid interface. Contact was not considered, although it has been dealt with in detail in previous work by the authors [20,21].

Firstly, two layers of uniformly distributed linear Timoshenko beam elements were used to model the specimen. One, ten, twenty and thirty spring pairs were used in the virtual crack closure technique to calculate the energy release rate partition G_I and G_{II}. The numerical energy release rate partitions for different values of M_2 are shown in Fig. 2 along with the Wang-Harvey Timoshenko and Euler beam partition theories. In the legend, the abbreviations '1 SP', '10 SP', etc. are used to indicate one and ten spring pairs being used in the calculation of G_I and G_{II}. It is seen that as the number of spring pairs is increased, the numerical partition closely approaches the Wang-Harvey Euler beam partition theory, which as has just been described, is also the Wang-Harvey *global* Timoshenko beam partition theory.

Secondly, six layers of uniformly distributed plane stress four-node quadrilateral (QUAD4) elements were used to model the specimen. Again, the energy release rate partition G_I and G_{II} was calculated using the virtual crack closure technique with one, ten, twenty and thirty spring pairs. The numerical energy release rate partitions for different values of M_2 are shown in Fig. 3 along with the Wang-Harvey Euler beam and averaged partition theories. As expected, as the numerical partition becomes a global one, it closely approaches the Wang-Harvey Euler beam partition theory.

Note that although in both cases thirty spring pairs represents a fairly large proportion of the length of the specimen, this is due to the discrete nature of the FEM. Using more elements along the length shows that a similarly converged global partition can be obtained over a shorter length.

4. Experimental validation

4.1. A note on mixed-mode failure criteria

Before reviewing experimental data from the literature and making comparative analyses, it is worth making some comments on mixed-mode failure criteria. In Section 4.2 and 4.3, some calculations and comparisons are made using the linear failure criterion, given by Eq. (59). Many different mixed-mode failure criteria have been suggested for predicting delamination growth. Reeder [28] gave a comprehensive review of them.

The linear failure criterion is the one most often used in the literature [28]. In addition there is a wealth of data that either strongly supports the criterion [34-39], or suggests criteria that are close to it [39-42].

Therefore, in this work, the linear failure criterion is expected to be reasonably accurate and to give a good approximation to the failure locus, against which different analytical partition theories can be compared. This is also the approach used by Charalambides et al. [26].

4.2. Asymmetric DCB test

The asymmetric DCB test is shown in Fig. 4 (a). Equal and opposite bending moments are applied to the upper and lower arms of an asymmetric beam specimen. The crack tip forces are therefore $M_{1B} = -M_{2B} = M$ and $N_{1Be} = 0$. Experimental measurements of the total critical energy release rate G_c for epoxy-matrix/carbon-fibre specimens with various values for h_1 and h_2 are given in Table 1 [26].

If the failure locus and critical energy release rates G_{Ic} and G_{IIc} for the material are known, then for a given partition theory the total critical energy release rate G_c for a specimen can be inferred. The linear failure locus is

$$\frac{G_I}{G_{Ic}} + \frac{G_{II}}{G_{IIc}} = 1 \tag{59}$$

As noted in Section 4.1, the actual failure locus is generally not far from this empirically suggested form [26]. Hashemi et al. [24] provide critical energy release rate values. From the DCB test $G_{Ic} = 0.27 \pm 0.015 \text{ kN/m}$; from the end-loaded split (ELS) test $G_{IIc} = 0.60 \pm 0.03 \text{ kN/m}$ and from the end-notched flexure (ENF) test $G_{IIc} = 0.65 \pm 0.02 \text{ kN/m}$. In this work the values used are: $G_{Ic} = 0.27 \text{ kN/m}$ and $G_{IIc} = 0.63 \text{ kN/m}$, which is an average of the two pure mode II tests and permitted by the error margins of both tests as well. From Eq. (59), the mode I energy release rate partition G_I/G_c from a given partition theory predicts the following total critical energy release rate G_c:

$$G_c = \left[\frac{\left(G_I/G_c\right)}{G_{Ic}} + \frac{1 - \left(G_I/G_c\right)}{G_{IIc}} \right]^{-1} \tag{60}$$

In Table 1, the G_c values predicted by the various partition theories in Section 2 for each specimen are compared against the experimentally measured G_c values. Both the Wang-Harvey

Euler beam theory and the Williams partition theory predict that the fracture is pure mode I for all values of h_1 and h_2. This is the $M_{2B}/M_{1B} = \theta_1'$ pure mode I mode [19,20]. Therefore $G_c = G_{Ic}$ for all the specimens. The experimental G_c values show very small variation. As the specimen thickness ratios γ changes from 1.33 to 4.11, the change in measured G_c is only 0.03 kN/m. Given that the error margin for G_{Ic} is 0.015 kN/m and the experimental G_c values are distributed evenly around 0.27 kN/m, the Wang-Harvey Euler beam and Williams theories are certainly both compatible with the experimental results.

The Wang-Harvey Timoshenko beam partition theory shows significantly more variation and in the majority of cases is not close to the experimental G_c values. In particular, for the thickest specimen for which $h = 10$ mm (the length is 120 mm, giving an aspect ratio of 12, which is very low), the measured G_c is not any closer to the value predicted by the Wang-Harvey Timoshenko beam partition theory. Since the Wang-Harvey Timoshenko beam theory might be expected to give a better prediction for low aspect ratios, this implies that perhaps the partition that determines failure is global and therefore given by the Wang-Harvey Euler beam partition theory. Observations from individual specimens must be treated with caution however and this possibility is far from conclusive.

The Suo-Hutchinson and averaged partition theories are very similar, as expected [20]. These two theories show a gradual increase in G_c with increasing γ, which is in agreement with the experimental results. Each result is also within the experimental error margin. It is therefore concluded that all theories, except the Wang-Harvey Timoshenko beam partition theory, are compatible with these experimental results. From this test, it is not possible to make further conclusions.

4.3. FRMM test

Fig. 4 (b) shows a test in which a bending moment M is applied to the upper arm only of an asymmetric beam specimen. The crack tip forces are therefore $M_{1B} = M$ and $M_{2B} = N_{1Be} = 0$, which produces a mixed mode. The total critical energy release rate G_c can be measured experimentally.

Charalambides et al. [26] took experimental measurements of G_c for multiple epoxy-matrix/carbon-fibre composite specimens, loaded in the fixed-ratio mixed-mode (FRMM) test, and partitioned them into G_I and G_{II}. The partition was made using the Williams partition theory. These values of G_I and G_{II} are the black, filled circle markers in Fig. 5. Since both the partition of G_c and the method by which it was partitioned are known, there is sufficient information to re-partition the data according to the different partition theories in Section 2.

First, the thickness ratio γ must be determined for each specimen. Because the total G_c is known from $G_I + G_{II}$, the critical load M_{1B} can be determined for each data point. Under this critical load and using the Williams partition theory, only one value of thickness ratio γ can give the G_I and G_{II} values. The thickness ratio γ of each specimen can therefore be calculated using Eq. (56) or Eq. (57). Now the experimentally measured G_c can be partitioned into G_I and G_{II} for each specimen, characterised by its thickness ratio γ, using the different partition theories in

Section 2. The Suo-Hutchinson partition and the three Wang-Harvey partitions are also presented in Fig. 5. The linear failure locus is also shown.

From Eq. (59), the importance of having a significant difference between G_{Ic} and G_{IIc} can be seen. If $G_{Ic} = G_{IIc}$, then the failure locus is not affected by the partition and all data points will lie on the linear failure locus regardless of the partition. However if $G_{Ic} \neq G_{IIc}$, then the partition *does* affect the failure locus. This has also been pointed out by Hashemi et. al. [27]. To assess the quality of the competing theories, it is therefore better to use a more brittle thermoset-matrix material, where there is usually a larger difference [26]. The epoxy-matrix/carbon-fibre composite specimens fulfil this requirement.

From Fig. 5, it is seen that the Wang-Harvey Euler beam partition theory performs much better than the other partition theories when compared with the linear failure locus. This could be because the specimens tested have a high aspect ratio (~27) and therefore essentially behave as Euler beams. As has been shown in Section 3, global measurements of G_c correspond to the Wang-Harvey Euler beam partition. Alternatively, it is also therefore possible that failure, at least in the experimental cases considered, is based on the Wang-Harvey global partition. It is not possible to distinguish which is the correct reason from these results. This latter possibility was also the conclusion of Charalambides et al. [26]. A trend line, which is represented by the black dashed line in Fig. 5, has been plotted through the Wang-Harvey Euler beam partition. For comparison, a solid black trend line has also been plotted through the Williams partition. For clarity, Fig. 6 shows the linear failure locus and these two data sets with their corresponding trend lines in isolation. It is seen that the Wang-Harvey Euler beam partition gives much closer agreement with the expected linear failure locus and expected G_{Ic} and G_{IIc} than the Williams partition. Quantitative statistical measures can also be given for better comparison. Comparing the Wang-Harvey Euler beam partition against the linear failure locus, the root mean square of the residuals is 0.025 kN/m. This is the 'standard error' or 'standard deviation'. For a normally distributed deviation, 68.3% of the data points would lie within one standard deviation of the linear failure locus and 95.5% within two standard deviations. For the Williams partition, the standard error (also against the linear failure locus) is 0.040 kN/m, which is 1.6 times greater than that from the Wang-Harvey Euler beam partition.

Now consider the other partition theories shown in Fig. 5. The Wang-Harvey Timoshenko beam partition of the experimental G_c measurements forms a separate vertical curve. The Suo-Hutchinson and the averaged partitions are very similar as expected and form another curve half way between the curves from the Wang-Harvey Euler and the Timoshenko beam partitions. Since the linear failure locus is generally regarded to be a good approximation to the actual failure locus, it must be concluded that, at least for these specimens, the Wang-Harvey *local* Timoshenko beam and averaged partition theories and the Suo-Hutchinson partition theory cannot give the partition that controls the fracture propagation. As stated above, there are two possible reasons for this. It might be because of the local nature of all these partition theories. If failure is dependent on the global partition then only the Wang-Harvey Euler beam partition theory can give the right partition. Alternatively, it could be because these specimens approach Euler beams in their behaviour because of their high aspect ratio.

Further evidence for the correctness of the Wang-Harvey Euler beam partition theory is given in Fig. 7. The figure responds to the inevitable question: if the Wang-Harvey Euler beam partition theory is the correct one and the linear failure locus is a good approximation, can it successfully predict the curve of the Williams partition? To answer the question, the Wang-Harvey Euler beam partition theory was used to calculate the thickness ratio γ for multiple points on the linear failure locus (the solid black line in the figure). Then the total critical energy

release rates G_c for these 'imaginary specimens' were repartitioned using the Williams partition theory. These partitions are represented by the black dashed line. The experimental values, partitioned using the two theories, are also shown. It is seen that the dashed line very closely predicts the curve of the Williams partition of the experimental measurements. Furthermore, the dashed line strongly resembles the 'general criterion for mixed mode failure' suggested by Charalambides et al. [26] on the basis of the Williams partition of the experimental results. This criterion is also plotted in figures in the paper by Hashemi et al. [27].

In summary, under the assumption that the linear failure locus is accurate, the Williams partition and his suggested failure criterion can be completely explained by using the Wang-Harvey Euler beam partition theory without resorting to correction factors for surface roughness and friction, as is done in Ref. [26]. In fact, if the Wang-Harvey Euler beam partition theory is correct, then the Williams partitions are exactly where they would be expected to be. It is proposed by the authors that the Wang-Harvey Euler beam partition theory offers the best and most simple explanation for all the observations, without having to propose extra mechanical effects.

Two additional sets of experimental data from the FRMM test are available from work by Hashemi et al. [27]. The first set of data is also for epoxy-matrix/carbon-fibre composite specimens. The Wang-Harvey Euler beam and Williams partitions of this experimental data with their trend lines and the linear failure locus are shown in Fig. 8. It is seen that the Wang-Harvey Euler beam partition is in excellent agreement with the linear failure locus. The standard error when compared with the linear failure locus is 0.018 kN/m. Once more, the Williams partition is not close to the linear failure locus. The standard error is 0.043 kN/m. The Suo-Hutchinson partition is not shown for clarity, but as before, it forms a curve approximately normal to the linear failure locus.

The second set of experimental data from Hashemi et al. [27] is for Polyether ether ketone (PEEK)-matrix/carbon-fibre composite specimens. There seems to be some significant variation in the literature for the critical energy release rates [24,27,28]. In this work the values from Hashemi et al. [24] are used. These values also appear to be the most reliable since they are directly from pure mode testing. Considering here only crack propagation (not initiation), from the DCB test $G_{Ic} = 2.42 \pm 0.016 \text{ kN/m}$ and from the ELS test $G_{IIc} = 3.16 \pm 0.014 \text{ kN/m}$. The Wang-Harvey Euler beam and Williams partitions of the experimental measurements are plotted in Fig. 9. Both partitions are approximately linear, very close to each other and far from the linear failure locus. The distance from the failure locus is likely to be due to values of critical energy release rate used, which are material constants and not determined by the partition theory. The uncertainty surrounding these values has already been pointed out. The fact that both partitions are close to each other and approximately linear is due to the critical energy release rates being very close to each other $G_{Ic}/G_{IIc} \approx 0.8$, which is in contrast to the epoxy-matrix/carbon-fibre composite specimens where $G_{Ic}/G_{IIc} \approx 0.4$. As pointed out above, when this is the case, although the individual partitions may be different, they will all lie on the same linear failure locus because the failure locus becomes

$$\frac{G}{G_{Ic}} = \frac{G}{G_{IIc}} = 1 \tag{61}$$

Therefore PEEK-matrix/carbon-fibre composite specimens are not suitable for assessing the quality of the competing theories. Donaldson [39] came to this same conclusion after experimental testing and comparisons with several mixed-mode fracture criteria.

4.4. Spalling test

Thouless et al. [23] investigated spalling in brittle plates. Spalling is where cracks occur very close to the surface, i.e. $\gamma \to \infty$. Fig. 10 shows the specimen and loading configuration. The spall, which has a thickness h_1 at the crack tip, is loaded axially by a force F, which is offset a distance d from the free surface. It therefore generally causes a tip bending moment as well. Eq. (62) describes the crack tip forces.

$$N_{1B} = -F \quad \text{and} \quad M_{1B} = F\left(\frac{h_1}{2} - d\right) \quad \text{and} \quad N_{2B} = M_{2B} = 0 \tag{62}$$

When the fracture propagates, it will propagate in pure mode I only in some direction [1,2,23]. As it propagates, it stabilises at a constant distance from the free surface. Thouless et al. described a series of experiments on PMMA and glass in which d is varied and the critical load and value of h_1 are determined. For convenience they introduced two quantities: the non-dimensional crack depth coefficient ξ

$$\xi = \frac{h_1}{d} \tag{63}$$

and the crack-loading coefficient Φ

$$\Phi = \frac{F}{b\sqrt{h_1}} \tag{64}$$

During stable propagation, the partition theories in Section 2 can be used to predict these values, which have been measured experimentally. Thouless et al. [23] used the Suo-Hutchinson partition (assuming a singular field). The resulting equations for the partition, rewritten as energy release rates for easier comparison with the other theories, are

$$G_{ISH} = \frac{F^2}{2b^2 dE\xi}\left[\sqrt{3}\sin\left(52.1^\circ\right) + \cos\left(52.1^\circ\right) - \frac{2\sqrt{3}}{\xi}\sin\left(52.1^\circ\right)\right]^2 \tag{65}$$

$$G_{IISH} = \frac{F^2}{2b^2 dE\xi}\left[\sin\left(52.1^\circ\right) - \sqrt{3}\cos\left(52.1^\circ\right) + \frac{2\sqrt{3}}{\xi}\cos\left(52.1^\circ\right)\right]^2 \tag{66}$$

Setting $G_{IISH} = 0$ allows ξ to be found. Substituting this value in Eq. (65) and using the relation given by Eq. (55) gives

$$\xi = 7.741 \quad \text{and} \quad \Phi = 0.869K_{Ic} \tag{67}$$

It is seen that ξ is independent of material properties whilst Φ is not. Thouless et al. [23] provided approximate values of for K_{Ic} for PMMA and for glass.

The Williams partition is as follows:

$$G_{IW} = \frac{3F^2\left(2-\xi\right)^2}{2b^2 dE\xi^3} \quad \text{and} \quad G_{IIW} = \frac{F^2}{2b^2 dE\xi} \tag{68}$$

For stable crack propagation with $G_{IISH} = 0$, the Williams partition theory requires that $\xi \to \infty$, i.e. an infinite thickness spall, which is obviously not valid for spalling when $\gamma \to \infty$ is assumed. To overcome this, Charalambides et al. [26] postulated an additional sliding component to G_{II} and derived a mixed-mode failure criterion based on the 'fracture surface roughness'.

The partitions from the three Wang-Harvey partition theories are given by Eqs. (69) to (71).

$$G_{IE} = \frac{3F^2\left(2 - 3\xi + \xi^2\right)}{b^2 dE\xi^3} \quad \text{and} \quad G_{IIE} = \frac{F^2\left(3 - \xi\right)}{b^2 dE\xi^2} \tag{69}$$

$$G_{IT} = \frac{3F^2\left(1 - \xi\right)^2}{2b^2 dE\xi^3} \quad \text{and} \quad G_{IIT} = \frac{F^2\left(3 - \xi\right)^2}{2b^2 dE\xi^3} \tag{70}$$

$$G_{IA} = \frac{3F^2(5 - 8\xi + 3\xi^2)}{4b^2 dE\xi^3} \quad \text{and} \quad G_{IIA} = \frac{F^2\left(9 - \xi^2\right)}{4b^2 dE\xi^3} \tag{71}$$

The values of ξ and Φ from the Hutchinson-Suo and Wang-Harvey partition theories for both materials are given in Table 2. The Wang-Harvey partition theories give the same results in this case, so are grouped together.

First, consider the crack-loading coefficient Φ. This is dependent on the critical mode I stress intensity factor K_{Ic}. From Thouless et al. [23], this is ~1.0 MPa-m$^{1/2}$ for PMMA, which is in agreement with the literature. Neither the Suo-Hutchinson nor the Wang-Harvey partition theories are in particularly good agreement with the measurement, although the value from the Wang-Harvey theories is the closest. However, the sensitivity of Φ to the value of ξ is noted. Using the Wang-Harvey Euler beam partition theory, if $\xi = 2.3$ instead of 3.0 then $\Phi = 2.1$, which is much closer to the measured value. For glass, Thouless et al. gave $K_{Ic} \approx 0.6$ MPa-m$^{1/2}$. Using this value, the value of Φ from the Wang-Harvey partition theories agrees quite well with the measured value. The Wang-Harvey partition theories again have better agreement than the Suo-Hutchinson one. However, other literature [43,44] quotes a higher value between 0.7 and 0.8 MPa-m$^{1/2}$. If the value of 0.75 MPa-m$^{1/2}$ from Ref. [43] is used then, as shown in Table 2, the Wang-Harvey partition theories are then exactly in agreement with the measured value of Φ.

Now consider the crack depth coefficient ξ. For all theories, this is independent of material properties. Experimentally, there is some variation between materials. As before, neither the Suo-Hutchinson values nor the values from the Wang-Harvey theories are very close to the measured values. For the PMMA specimens, the Wang-Harvey partitions are the closest with 37.5% discrepancy, and for glass, the Suo-Hutchinson partition is the closest with 29% discrepancy. Thouless et al. [23] published a photograph of three spalled specimens of PMMA. These are reproduced with permission in Fig. 11. They are potentially revealing because a scale is given and values of d and h_1 can be measured from the photograph. Note that the load was evenly applied to an elevated region on the specimen, so d is half the thickness of this elevated region. Black lines have been added over the specimens in Fig. 11 to indicate the regions over which d and h_1 were averaged. From left to right, the measured values of ξ are 3.5, 3.4 and 3.9, which are significantly less than the value of 4.8 given by Thouless et al. and much closer to the value predicted by the Wang-Harvey partition theories. This photograph was presented by Thouless et al. to indicate the consistency of the measured ξ values. Therefore these measurements should

be representative of the whole sample of experimental measurements. No photographs are available for the glass. The authors are planning to replicate the experiments of Thouless et al. to either confirm or refute the possibility raised above.

Overall, it can be concluded that the Wang-Harvey partition theories perform better than the Suo-Hutchinson and Williams partition theories in modelling this test. Observed discrepancies can be explained, but further experimental data is needed to confirm these explanations.

5. Conclusions

The performance of five different partition theories has been investigated by using experimental results from the literature for a range of tests. The partition theories used are the Williams theory [3], the Suo-Hutchinson theory [5-7] and the Wang-Harvey partition theories of the authors [19-21], based on the Euler and Timoshenko beam theories.

The Wang-Harvey Euler partition theory offers the best and most simple explanation for all the experimental observations. There are two possible reasons for this:

1. The aspect ratios of the specimens, which have been tested, are high enough for their behaviour to be essentially that of Euler beams. The most suitable partition theory would therefore be the Wang-Harvey Euler beam partition theory. If this is correct, then for some specimens the Wang-Harvey Timoshenko beam or averaged partition theories might provide the best result. This seems less likely though because for the thicker specimens tested, where the through-thickness shear effect is greater, there is no tendency towards the Wang-Harvey Timoshenko beam partition.
2. The global partition from the Wang-Harvey partition theories, which has been shown to be equal to the Wang-Harvey Euler beam partition, is the one that determines failure.

All the partition theories, except the Wang-Harvey Timoshenko beam partition theory, are compatible with the results of the asymmetric DCB test, due to the error margin of the measurements. No further conclusions were possible from this test. For the FRMM test, the Wang-Harvey Euler beam partition theory partitions the measurements of the total G_c so that the resulting G_I and G_{II} closely follow the expected linear failure locus. Under the assumption that the linear failure locus is accurate, the Williams partition and his suggested failure criterion can be completely explained by using the Wang-Harvey Euler beam partition theory. No recourse to extra mechanical effects, such as fracture roughness and friction is required. In fact, if the Wang-Harvey Euler beam partition theory is correct, then the Williams partitions are exactly where they would be expected to be. For this test, the other partition theories give very different partitions and form curves approximately normal to the linear failure locus.

Finally, this paper has looked at results from spalling tests. In these tests, the spall stabilises at a constant distance from the free surface, allowing these interfacial partition theories to be used, and propagates in pure mode I. The Wang-Harvey theories all predict the same crack depth and energy release rate. Generally, these theories give better agreement with the measured values than the Suo-Hutchinson partition theory. In some cases, values from the Wang-Harvey theories are in very close agreement with the measured values. When this is not the case, plausible explanations are offered. First the crack-loading coefficient Φ is particularly sensitive to the crack depth, represented by ξ. A small change in ξ can reconcile the value of Φ predicted by the Wang-Harvey theories with the measured value. In addition, by examining scaled photos of the spalled specimens, there appears to be a discrepancy between the measured and quoted values of ξ in Ref. [23]. Measurements from the photos by the authors give much better agreement with the values from the Wang-Harvey partition theories.

Acknowledgement

The authors are very grateful to Prof. J. Hutchinson of Harvard University for helpful discussion regarding the work and also for giving permission for a figure from Ref. [23] to be reproduced. The authors are also very grateful to the reviewers for their helpful comments.

References

1. Gol'dstein RV, Salganik RL. Brittle fracture of solids with arbitrary cracks. Int J Fract 1974;10:507-23.
2. Cotterel B, Rice JR. Slightly curved or kinked cracks. Int J Fract 1980;16:155-69.
3. Williams JG. On the calculation of energy release rates for cracked laminates. Int J Fract Mech 1988;36:101-19.
4. Schapery RA, Davidson BD. Prediction of energy release rate for mixed-mode delamination using classical plate theory. Appl Mech Rev 1990;43:S281-7.
5. Suo Z. Delamination specimens for orthotropic materials. J Appl Mech 1990;56:627-34.
6. Suo Z, Hutchinson JW. Interface crack between two elastic layers. Int J Fract 1990;43:1-18.
7. Hutchinson JW, Suo Z. Mixed mode cracking in layered materials. Adv Appl Mech 1992;29:63-191.
8. Bruno D, Greco F. Mixed mode delamination in plates: a refined approach. Int J Solids Struct 2001;38:9149-77.
9. Wang J, Qiao P. Interface crack between two shear deformable elastic layers. J Mech Phys Solids 2004;52:891-905.
10. Nguyen C, Levy AJ. An exact theory of interfacial debonding in layered elastic composites. Int J Solids Struct 2009;46:2712-23.
11. Yan Y, Shang F. Cohesive zone modelling of interfacial delamination in PZT thin films. Int J Solids Struct 2009;46:2739-49.
12. Ouyang Z, Li G. Nonlinear interface shear fracture of end notched flexure specimens. Int J Solids Struct 2009;46:2659-68.
13. Zou Z, Reid SR, Li S, Soden PD. General expressions for energy release rates for delamination in composite laminates. Proc R Soc Lond A 2002;458:645-67.
14. Li S, Reid SR, Zou Z. Modelling damage of multiple delaminations and transverse matrix cracking in laminated composites due to low velocity lateral impact. Compos Sci Technol 2005;66:827-36.
15. Wang S, Harvey C. Fracture mode partition rules for DCB. 17th Interactional Conference on Composite/Nano Engineering (ICCE-17), July 2009, Honolulu, Hawaii, USA.
16. Harvey C, Wang S. Modelling of delamination propagation in composite laminated beam structures. Proceedings of the 7th International Conference of Computational Methods in Science and Engineering (ICCMSE 2009), Simos T E (ed), American Institute of Physics, Rhodes, Greece.
17. Wang S, Harvey C. Mixed mode partition in one dimensional fracture. Journal of Key Engineering Materials 2011;462-63:616-21. Also a plenary lecture in the 8th International Conference on Fracture and Strength of Solids (FEOFS 2010), 7-9th June 2010, Kuala Lumpur, Malaysia.
18. Wang S, Guan L. On fracture mode partition theories, Computational Material Sciences 2012;52:240-45.

19. Wang S, Harvey C. A theory of one-dimensional fracture. Compos Struct 2012;94:758-67. Also a plenary lecture at the 16th International Conference on Composite Structures (ICCS16), 28-30th June 2011, Porto, Portugal.
20. Wang S, Harvey C. Mixed mode partition theories for one dimensional fracture. Eng Fract Mech 2012;79:329-52.
21. Harvey C, Wang S. Mixed-mode partition theories for one-dimensional delamination in laminated composite beams. Eng Fract Mech. (under review)
22. Thouless MD. Fracture of a model interface under mixed mode loading. Acta Metall Mater 1990;38:1135-40.
23. Thouless MD, Evans AG, Ashby MF, Hutchinson JW. The edge cracking and spalling of brittle plates. Acta Metall 1987;35:1333-41.
24. Hashemi S, Kinloch AJ, Williams JG. The analysis of interlaminar fracture in uniaxial fibre-polymer composites. Proc R Soc Lond A 1990;427:173-99.
25. Kinloch AJ, Wang Y, Williams JG, Yayla P. The mixed-mode delamination of fibre composite materials. Compos Sci Technol 1993;47:225-37.
26. Charalambides M, Kinloch AJ, Wang W, Williams JG. On the analysis of mixed-mode failure. Int J Fract 1992;54:269-91.
27. Hashemi S, Kinloch AJ, Williams G. Mixed-mode fracture in fiber-polymer composite laminates. In: O'Brien TK, editor. Composite materials: fatigue and fracture (third volume), ASTM STP 1110. Philadelphia, PA: American Society for Testing and Materials, 1991. p. 143-68.
28. Reeder JR. An evaluation of mixed-mode delamination failure criteria. NASA Technical Memorandum 104210. Hampton, VA: Langley Research Center, 1992.
29. Li S. Rigidities of one-dimensional laminates of composite materials. J Eng Mech 1996;122:371-74.
30. Li S, Lim S-H. Variational principles for generalised plane strain problems and their applications. Composites Part A 2005;36:353-65.
31. Rice JR. A path independent integral and the approximate analysis of strain concentration by notches and cracks. J Appl Mech 1968;35:379-86.
32. Cui W, Wisnom M. A combined stress-based and fracture-mechanics based model for predicting delamination in composites. Composites 1993;24:467-74.
33. Rybicki EF, Kanninen MF. A finite element calculation of stress intensity factors by a modified crack closure integral. Eng Frac Mech 1977;9:931-8.
34. Zhang Y, Wang S. Buckling, post-buckling and delamination propagation in debonded composite laminates. Part 1: Theoretical development. Compos Struct 2009;88:121-30 Also, a plenary lecture in the 16th International Conference on Composite/Nano Engineering (ICCE-16), July 2008, Kunming, China.
35. Wang S, Zhang Y. Buckling, post-buckling and delamination propagation in debonded composite laminates. Part 2: Numerical applications. Compos Struct 2009;88:131-46 Also, a plenary lecture in the 16th International Conference on Composite/Nano Engineering (ICCE-16), July 2008, Kunming, China.
36. Kutlu Z, Chang F-K. Composite panels containing through-the-width delaminations and subjected to compression. Part II: experiments and verification. Compos Struct 1995;31:297-314.
37. Jurf RA, Pipes RB. Interlaminar fracture of composite materials. J Comp Mater 1982;16:386-94.

38. Sanford RJ, Stonesifer FR. Fracture toughness of filament-wound composites. Part 1: Effect of material variables. Naval Research Laboratory 1970. NRL Report 7112.
39. Donaldson SL. Fracture toughness testing of graphite/epoxy and graphite/PEEK composites. Composites 1985;16:103-112.
40. Wu EM. Application of fracture mechanics to anisotropic plates. J Appl Mech 1967;34:967-74.
41. McKinney JM. Mixed-mode fracture of unidirectional graphite/epoxy composites. J Comp Mater 1972;6:164-6.
42. Yoon SH, Hong CS. Interlaminar fracture toughness of graphite/epoxy composite under mixed-mode deformations. Exp Mech 1990;30:234-39.
43. Anstis GR, Chantikul P, Lawn BR, Marshall DB. A critical evaluation of indentation techniques for measuring fracture toughness. J Am Ceram Soc 1981;64:533-8.
44. Dowling NE. Mechanical behavior of materials: engineering methods for deformation, fracture, and fatigue. Englewood Cliffs, NJ: Prentice Hall, 1993. p. 283.

Figure captions

Fig. 1: A DCB (a) general description (b) crack tip forces.
Fig. 2: Analytical and numerical Timoshenko beam partitions of local and global energy release rate G_1/G of a DCB with varying M_2 and $M_1 = 1$.
Fig. 3: Analytical and numerical 2D elasticity partitions of local and global energy release rate G_1/G of a DCB with varying M_2 and $M_1 = 1$.
Fig. 4: Tests with asymmetric beam specimens (a) Asymmetric DCB test (b) FRMM test.
Fig. 5: A comparison of the FRMM test [26] partitions from various partition theories and the linear failure locus for epoxy-matrix/carbon-fibre composite specimens.
Fig. 6: A comparison of the FRMM test [26] partitions from the Williams and Wang-Harvey Euler beam partition theories and the linear failure locus for epoxy-matrix/carbon-fibre composite specimens.
Fig. 7: The linear failure locus for epoxy-matrix/carbon-fibre composite specimens repartitioned using the Wang-Harvey Euler beam partition theory into the expected Williams partition curve and the FRMM test [26] partitions from the corresponding partition theories.
Fig. 8: A comparison of the FRMM test [27] partitions from the Williams and Wang-Harvey Euler beam partition theories and the linear failure locus for epoxy-matrix/carbon-fibre composite specimens.
Fig. 9: A comparison of the FRMM test [27] partitions from the Williams and Wang-Harvey Euler beam partition theories and the linear failure locus for PEEK-matrix/carbon-fibre composite specimens.
Fig. 10: Spalling in a brittle plate with an offset load.
Fig. 11: Optical views of spalled segments of PMMA [23].

Table captions

Table 1: Values of measured critical energy release rate G_c for an epoxy carbon-fibre composite asymmetric DCB together with the values expected from the various partition theories.

Table 2: Crack-loading coefficient $\Phi \left(\mathrm{MPa}\sqrt{\mathrm{m}} \right)$ and crack depth coefficient ξ propagation constants from the various partition theories for the spalling of brittle plates.

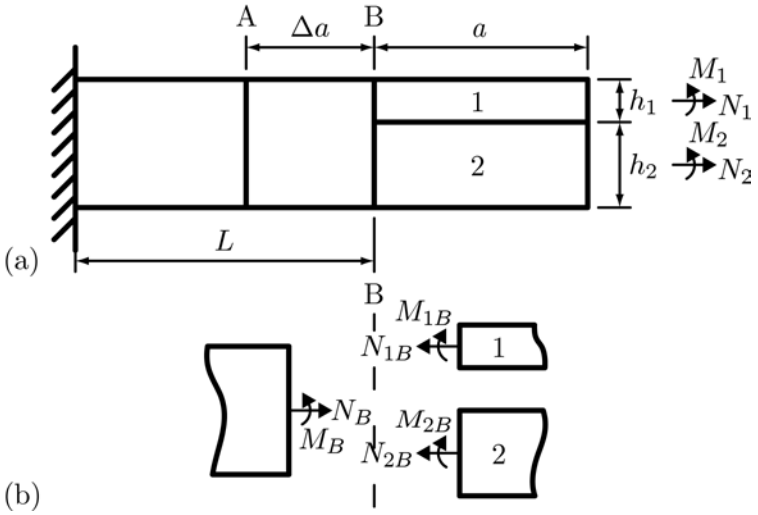

Fig. 1: A DCB (a) general description (b) crack tip forces.

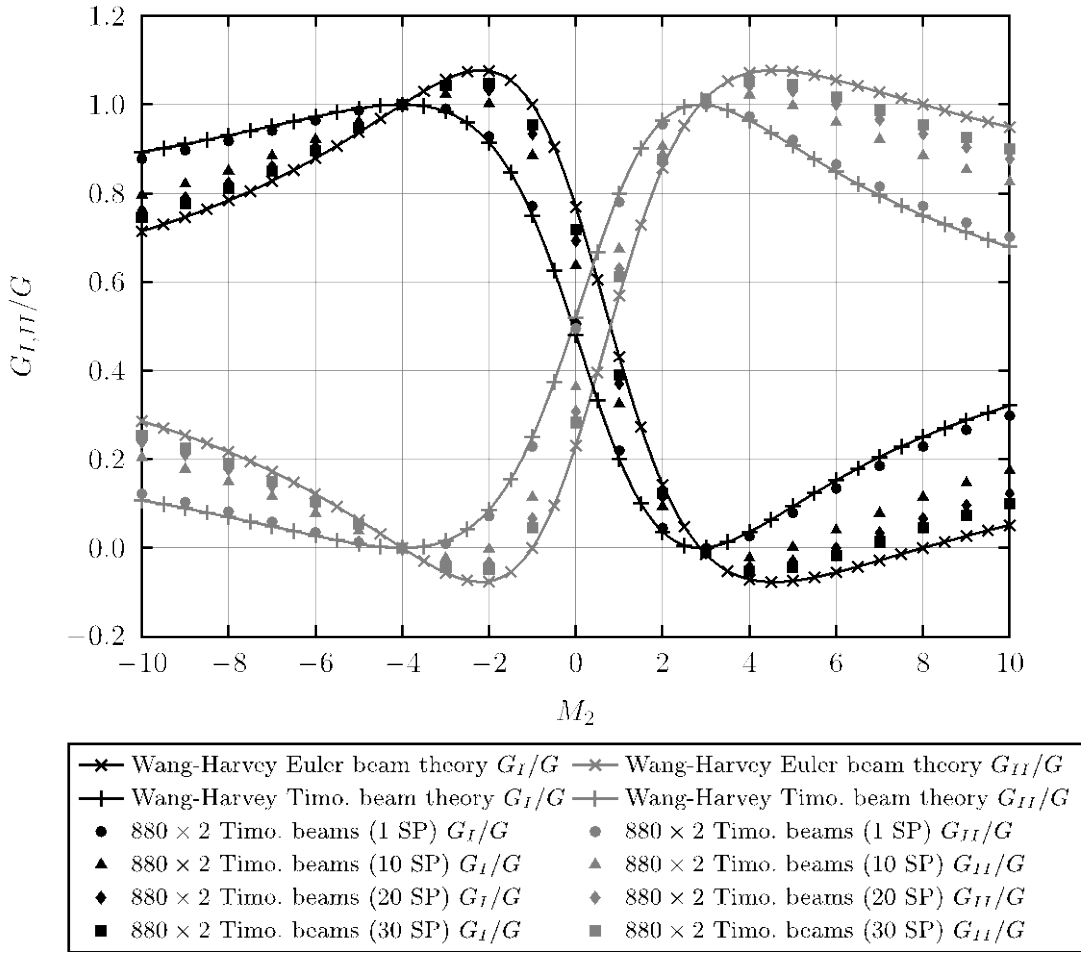

Fig. 2: Analytical and numerical Timoshenko beam partitions of local and global energy release rate G_I/G of a DCB with varying M_2 and $M_1 = 1$.

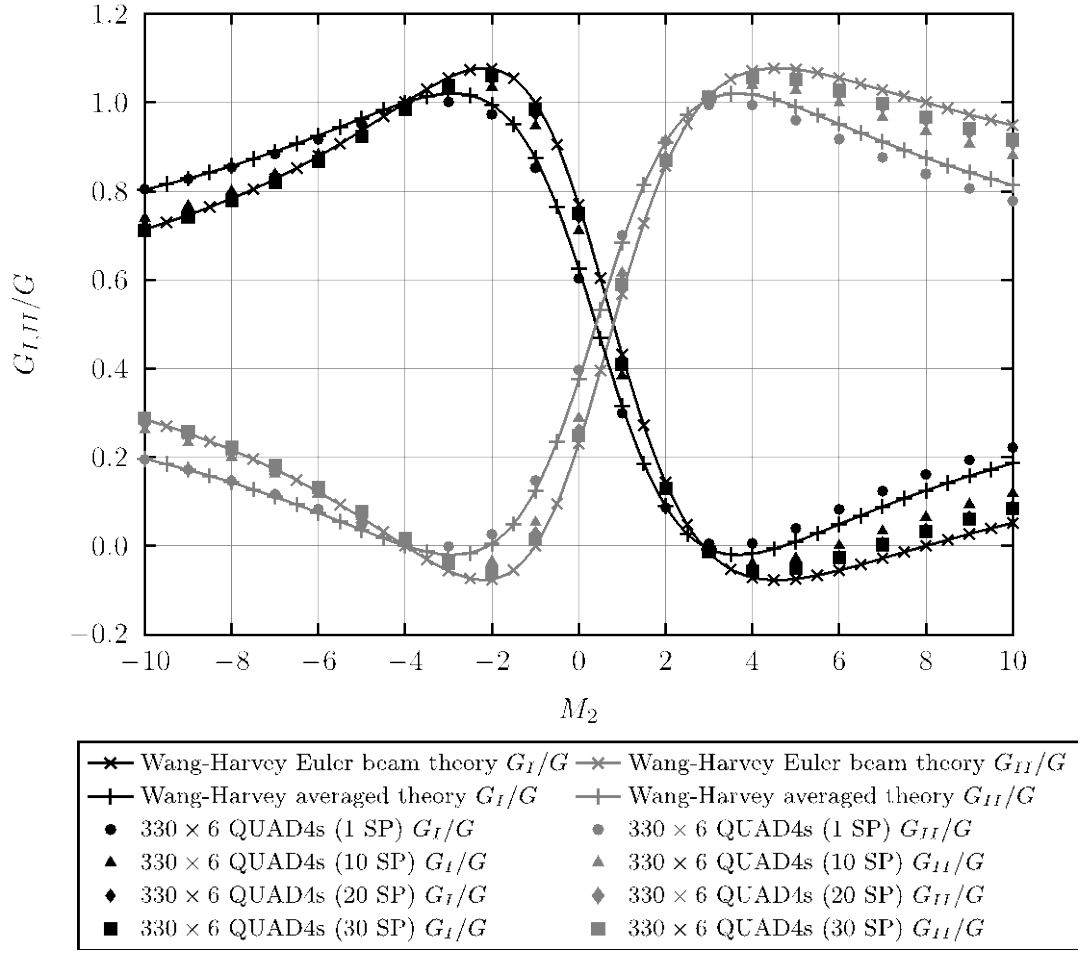

Fig. 3: Analytical and numerical 2D elasticity partitions of local and global energy release rate G_I/G of a DCB with varying M_2 and $M_1 = 1$.

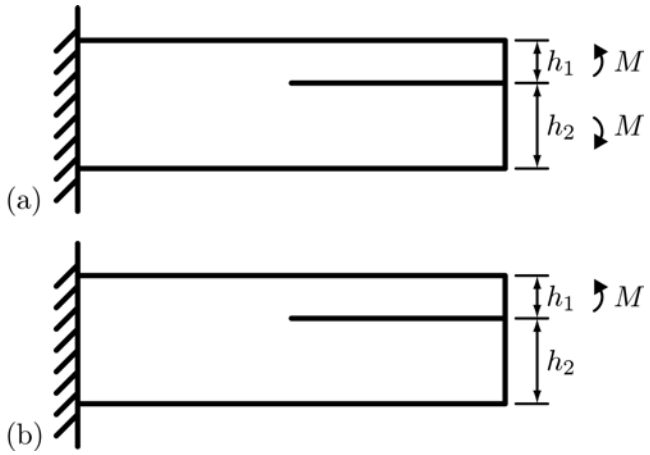

Fig. 4: Tests with asymmetric beam specimens (a) Asymmetric DCB test (b) FRMM test.

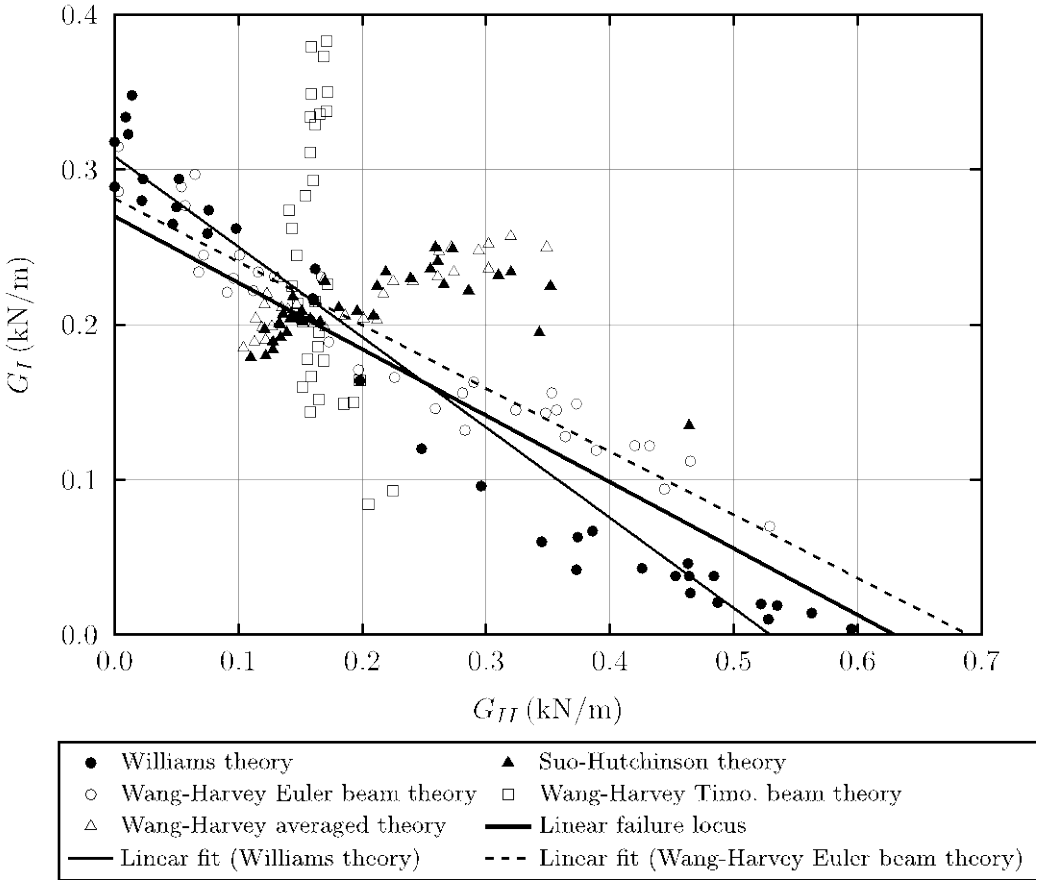

Fig. 5: A comparison of the FRMM test [26] partitions from various partition theories and the linear failure locus for epoxy-matrix/carbon-fibre composite specimens.

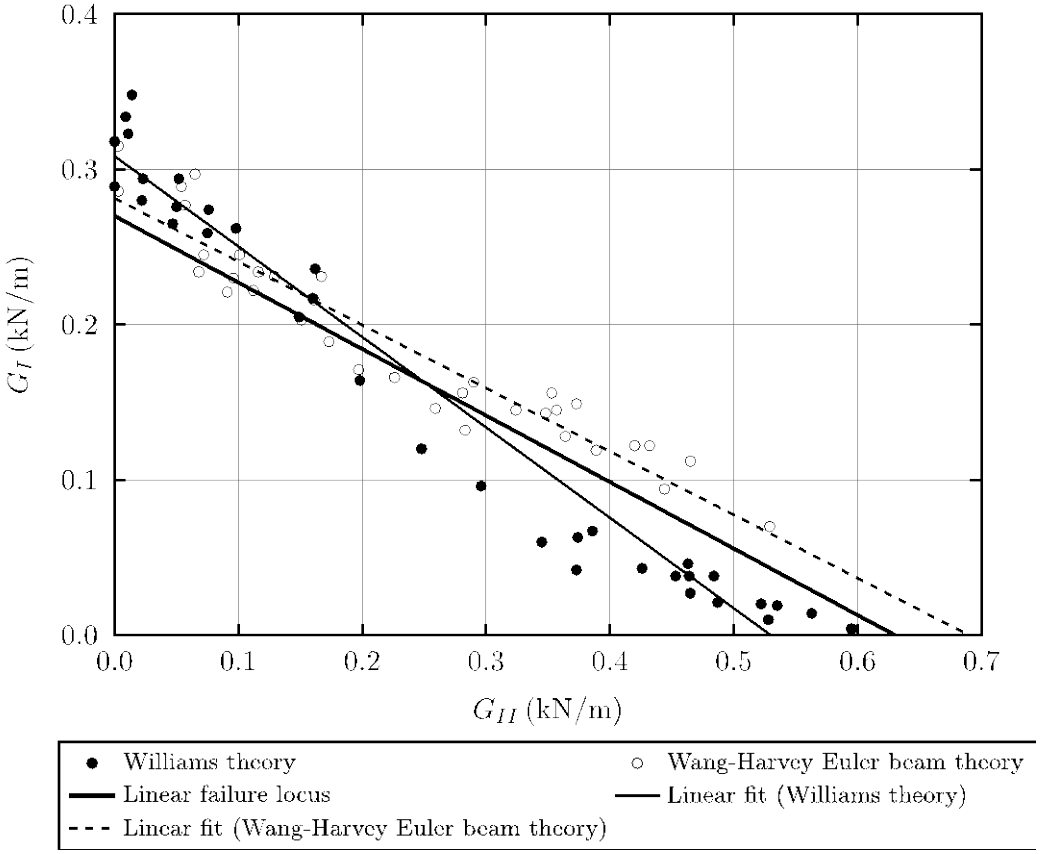

Fig. 6: A comparison of the FRMM test [26] partitions from the Williams and Wang-Harvey Euler beam partition theories and the linear failure locus for epoxy-matrix/carbon-fibre composite specimens.

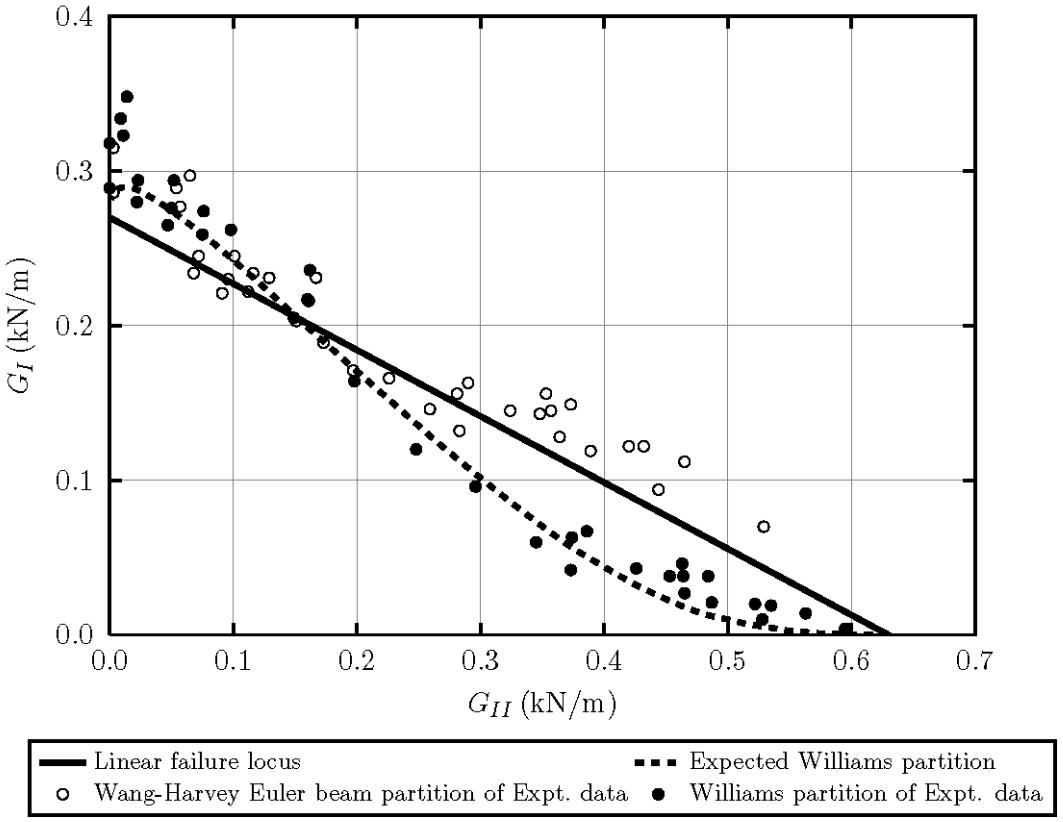

Fig. 7: The linear failure locus for epoxy-matrix/carbon-fibre composite specimens repartitioned using the Wang-Harvey Euler beam partition theory into the expected Williams partition curve and the FRMM test [26] partitions from the corresponding partition theories.

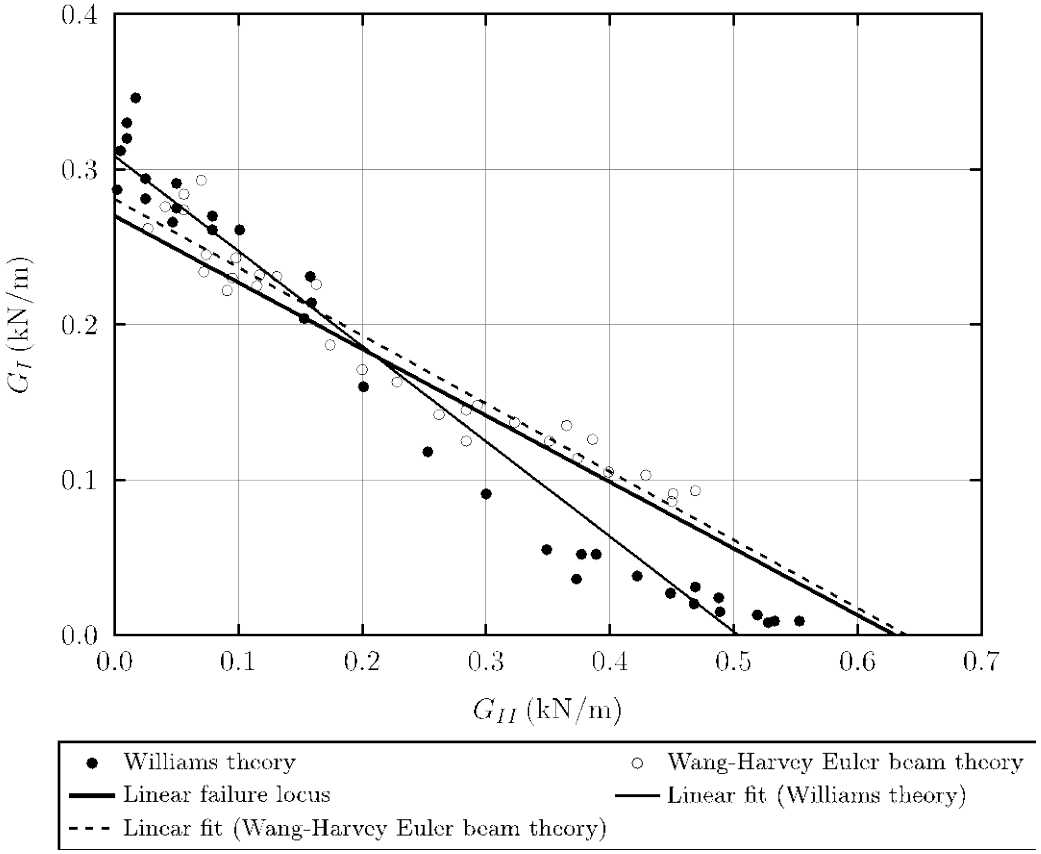

Fig. 8: A comparison of the FRMM test [27] partitions from the Williams and Wang-Harvey Euler beam partition theories and the linear failure locus for epoxy-matrix/carbon-fibre composite specimens.

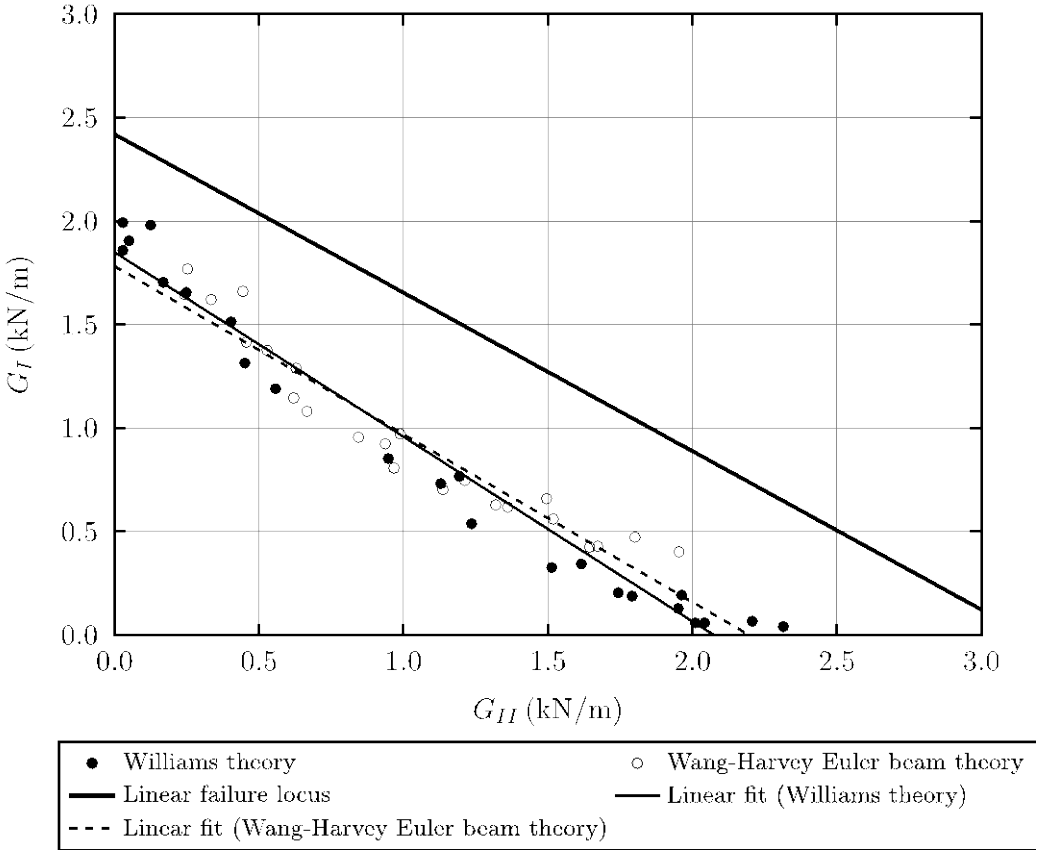

Fig. 9: A comparison of the FRMM test [27] partitions from the Williams and Wang-Harvey Euler beam partition theories and the linear failure locus for PEEK-matrix/carbon-fibre composite specimens.

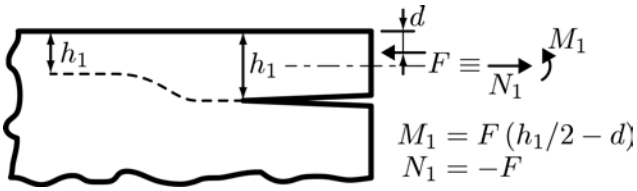

Fig. 10: Spalling in a brittle plate with an offset load.

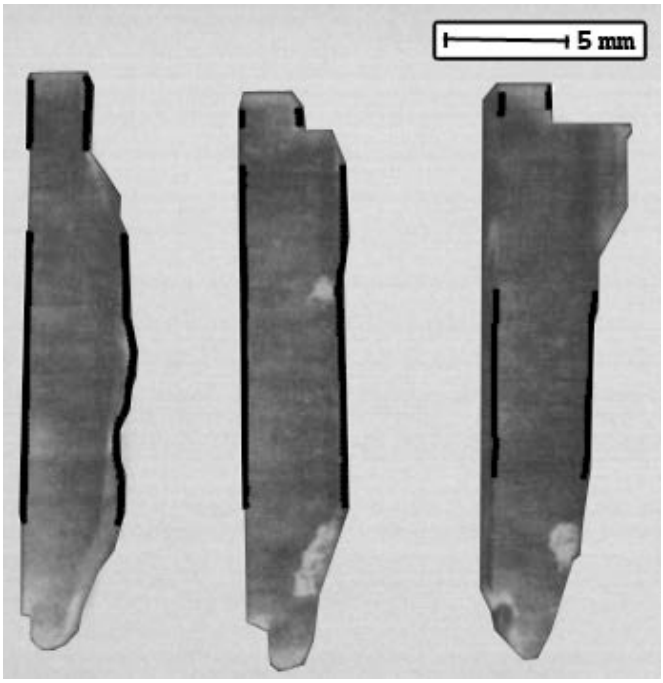

Fig. 11: Optical views of spalled segments of PMMA [23].

Table 1: Values of measured critical energy release rate G_c for an epoxy carbon-fibre composite asymmetric DCB together with the values expected from the various partition theories.

							Wang-Harvey theories					
	Measured		Suo-Hutchinson		Williams		Euler		Timoshenko		Averaged	
γ	h (mm)	G_c $(\mathrm{kN/m})$	G_f/G $(\%)$	G_c $(\mathrm{kN/m})$	G_f/G $(\%)$	G_c $(\mathrm{kN/m})$	G_f/G $(\%)$	G_c $(\mathrm{kN/m})$	G_f/G $(\%)$	G_c $(\mathrm{kN/m})$	G_f/G $(\%)$	G_c $(\mathrm{kN/m})$
1.33	3.85	0.26	96.4	0.28	100.0	0.27	100.0	0.27	94.2	0.28	97.1	0.27
1.55	3.70	0.27	92.4	0.28	100.0	0.27	100.0	0.27	87.7	0.29	93.9	0.28
1.97	3.33	0.28	85.5	0.29	100.0	0.27	100.0	0.27	75.7	0.31	87.8	0.29
3.72	10.00	0.29	75.3	0.31	100.0	0.27	100.0	0.27	50.1	0.38	75.1	0.31
4.11	2.86	0.29	75.2	0.31	100.0	0.27	100.0	0.27	47.4	0.39	73.7	0.32

Table 2: Crack-loading coefficient $\Phi\ \left(\mathrm{MPa}\sqrt{\mathrm{m}}\right)$ and crack depth coefficient ξ propagation constants from the various partition theories for the spalling of brittle plates.

		Measured		Suo-Hutchinson		Wang-Harvey theories (all the same here)	
Material	K_{Ic}	Φ	ξ	Φ	ξ	Φ	ξ
PMMA	~1.0	2.4	4.8	~0.87	7.74	~1.22	3.0
Glass	~0.6	0.9	6.0	~0.52	7.74	~0.73	3.0
"	~0.75	0.9	"	~0.64	"	~0.91	"